Spectral features of SKR observed by Cassini/RPWS: Frequency bandwidth, flux density and polarization

Patrick H. M. Galopeau, Mohammed Y. Boudjada, Alain Lecacheux

Spectral features of SKR observed by Cassini/RPWS: Frequency bandwidth, flux density and polarization

Patrick H. M. Galopeau,[1] Mohammed Y. Boudjada,[2] and Alain Lecacheux[3]

Received 30 May 2007; revised 15 July 2007; accepted 11 September 2007; published 20 November 2007.

[1] We report on an analysis about the spectral shape of the Saturnian kilometric radiation (SKR) recorded by the RPWS/HFR experiment onboard the Cassini spacecraft. The SKR envelope is found to be very variable in timescales covering a large range, from hours to days. Despite this change, we proceed to a classification of the shape in the frequency range from 3.5 kHz to 1.2 MHz taking into consideration the phenomenology and the state polarization of the radio wave. In the considered SKR bandwidth, we make a distinction between three principal components having different spectral shapes and degrees of total polarization. The well-known SKR component exhibits a degree of circular polarization close to 100% and emits in the frequency range from 80–90 kHz to 800–900 kHz. The two other components become visible in the lower and higher parts of the HFR receiver and show a weak linear polarization less than 10%. The generation of the SKR is linked to particles precipitations in the auroral regions, nevertheless the variability of the spectral shape is still subject of investigation. The present analysis is confronted with the theoretical model of SKR envelope spectrum proposed by Galopeau et al. (1989).

Citation: Galopeau, P. H. M., M. Y. Boudjada, and A. Lecacheux (2007), Spectral features of SKR observed by Cassini/RPWS: Frequency bandwidth, flux density and polarization, *J. Geophys. Res.*, *112*, A11213, doi:10.1029/2007JA012573.

1. Introduction

[2] The Saturnian kilometric radiation (SKR) was discovered more than twenty-five years ago by the Planetary Radio Astronomy experiment on board the Voyager spacecraft [*Kaiser et al.*, 1980]. It is an intense polarized nonthermal radio emission, the spectrum of which peaks near 200 kHz and extends from about 3 kHz to more than 1.2 MHz [*Kaiser et al.*, 1984]. The radiation intensity is modulated by the planetary rotation and shows evidence of long-term variability at about 25-day period attributed to the influence of the solar wind on the Saturnian magnetosphere [*Desch*, 1982; *Desch and Rucker*, 1983]. The SKR was principally observed by the two Voyager spacecraft in a very limited angle of view with almost no latitudinal coverage [*Genova*, 1985]. The emission source was determined to be fixed in local time (near 1030 LT) and at relatively high magnetic latitude [see *Galopeau*, 1992, and references therein]. The Cassini mission offers the opportunity to re-investigate the physical characteristics of Saturn's magnetosphere and to provide responses to some unambiguous enquires, like the origin of the shape of the SKR spectrum, the source location and the planetary rotation period.

[3] It is well-known that the cyclotron maser instability [hereafter CMI, *Wu and Lee*, 1979] was proposed as a common mechanism at the origin of the various nonthermal planetary radio emissions. This mechanism leads to a direct strong amplification of the waves from an electron distribution precipitating in regions of high latitude along magnetic field lines. Despite this common generation mechanism and their numerous common properties, the planetary radio emissions display in the meantime different spectral features; it is particularly the case for those coming from the Earth, Jupiter and Saturn [*Kaiser and Desch*, 1984] which have been studied for a long time. These changes from one planet to another can be mainly explained by the rotation period of the planet, the magnetic field topology, how the latter interacts with the incident solar wind, and also by the influence of the natural satellites. In the case of the Jovian emissions, first detected more than 50 years ago [*Burke and Franklin*, 1955] and extensively studied from ground-based and spacecraft observations, the phenomenology exhibits several kinds of spectral features. The Jovian dynamic spectrum reveals large [*Lecacheux et al.*, 1998] and narrow structures with timescales from millisecond to several hours [*Boudjada and Genova*, 1991; *Boudjada et al.*, 2000]. In general the origin of the spectral shape, and in particular that of the maximum spectrum, is poorly known and cannot be directly derived from Wu and Lee's theory. Hence the maximum observed frequency is found to be close to the maximum gyrofrequency at the surface of the planet as predicted from the CMI theory [*Genova and Aubier*, 1987]. However, the origin of the lowest observed frequency of the radio waves is not clearly explained,

[1] CETP/UVSQ/IPSL, CNRS UMR 8639, Vélizy, France.
[2] Space Research Institute, Austrian Academy of Sciences, Graz, Austria.
[3] Observatoire de Paris, CNRS UMR 8109, Meudon, France.

0148-0227/07/2007JA012573

principally because it is generated far from the planetary surface, in a region where the magnetic field lines diverge.

[4] *Genova et al.* [1983] reported an analysis of the spectral envelope of the Saturnian kilometric radiation recorded by the Voyager/PRA experiment about one month around the encounters. The SKR dynamic spectra vary from the lowest PRA frequency channel (i.e., 1 kHz) to more than 100 kHz and the highest frequency is found between ~500 kHz and more than 1 MHz. *Galopeau et al.* [1991] reported that the maximum frequency for the northern and southern hemispheres are about 1.2 MHz and 900 kHz, respectively. No clear periodicity was established from the variation of the lower and upper limits of the SKR envelope over several consecutive rotations. Using averaged spectra over one Saturnian rotation, *Genova et al.* [1983] classified the SKR emissions in three kinds: (a) 'high-frequency wide spectrum', (b) 'low-frequency steep spectrum', and (c) 'complex spectrum' which seems to be the superposition of both previous kinds of radiations. *Warwick et al.* [1982] found that the intensity spectrum over a long period is dominated by the first and the second kinds of spectrum during the Voyager out- and in-bound, respectively. Also a theoretical model of SKR spectrum, based on the CMI generation mechanism in an inhomogeneous medium, was calculated by *Galopeau et al.* [1989]. A theoretical envelope spectrum was computed using this model that shows the role of several plasma key parameters (like the electronic density and the magnetic field) in the source region. Nevertheless the global SKR envelope is still subject of investigation in particular because the upper and the lower frequency limits have unlike origins. The upper limit depends mainly on the plasma and electron cyclotron frequencies in the source [*Galopeau et al.*, 1991] whereas the lower limit seems to be linked principally to the plasma density, and to be under the influence of the solar wind. This was noticed during the immersion of Saturn in Jupiter's magnetospheric tail [*Kurth et al.*, 1981b]. An effect of the satellite Dione was also proposed [*Kurth et al.*, 1981a].

[5] In this paper, we attempt to characterize the SKR envelope as recorded by the Cassini/RPWS experiment during the orbits 19 and 20 of the spacecraft around the planet. In the next section we describe the RPWS reception system, in particular the high frequency receiver (HFR) and the antenna configuration, and we summarize the main steps toward the data calibration. In section 3, we investigate the spectral shape of Saturn's kilometric radiation and emphasis on the analysis of three key factors: the flux density, the frequency bandwidth, and the polarization. The main outcomes are discussed in section 4 and combined to recent and previous investigations initiated by the Cassini and Voyager missions. A summary of the main results and the future investigations are presented in the last section.

2. Cassini/RPWS Experiment

2.1. High Frequency Receiver

[6] The RPWS experiment is designed to measure the electric and magnetic fields of radio emissions and plasma waves across a broad range of frequencies [*Gurnett et al.*, 2004]. The high frequency receiver (hereafter HFR) enables the analysis of incoming radio waves by combining signals from three 10-m long antenna elements, labeled E_U, E_V and E_W. Two elements (E_U and E_V) are mounted with an angle of 120° between them, and the third one (E_W) is mounted perpendicular to the plane formed by the two previous elements.

[7] For our investigations, we consider the so-called 'dipole mode' antenna configuration where two signals are mixed: the first one (E_X) is taken from the difference between the voltages on E_U and E_V, and the second one (E_Z) is derived from the E_W antenna voltage. The HFR instrument provides simultaneous auto- and cross-correlation measurements from two selected antennas over a frequency range from 3.5 kHz to 16 MHz. This receiver leads to measure the arrival direction of radio waves and also their corresponding Stokes parameters by combining the signals detected by the monopole electric antennas. The HFR instrument is divided into five distinct subsets: band A (3.5–16 kHz), band B (16–71 kHz), band C (71–319 kHz), HF1 (0.1–4.125 MHz) and HF2 (1.25–16.125 MHz). The intrinsic noise level is lower than 5×10^{-17} V^2 m^{-2} Hz^{-1} and the sensitivity is mostly limited by the galactic background level for frequencies above 100 kHz [*Lecacheux*, 2001].

2.2. Polarization Measurements

[8] Through real time computation of correlation products of instantaneous E_X and E_Z antenna voltage outputs (i.e., $[\langle E_X E_X^\star\rangle, \langle E_X E_Z^\star\rangle, \langle E_X^\star E_Z\rangle, \langle E_Z E_Z^\star\rangle]$), the Cassini/RPWS instrument provides indirect measurements of the four Stokes parameters of the radio wave, i.e., its flux density S and its linear (SQ, SU) and circular SV polarization components. The actual measurements S_A, S_AQ_A, S_AU_A, S_AV_A define the 'apparent' polarization, which results from the antenna directivity patterns. From general principle of optics, it can easily be shown that the relationship between 'apparent' and 'true' Stokes parameters (for example, [*Hamaker et al.*, 1996] for a general application to ground based radioastronomy, or [*Lecacheux*, 2005] for application to space radioastronomy) is basically a linear relationship, i.e.:

$$\mathbf{\Sigma}_A = \mathbf{M} \cdot \mathbf{\Sigma},$$

$$\text{where } \mathbf{\Sigma}_A = \begin{bmatrix} S_AQ_A \\ S_AU_A \\ S_AV_A \\ S_A \end{bmatrix} \text{ and } \mathbf{\Sigma} = \begin{bmatrix} SQ \\ SU \\ SV \\ S \end{bmatrix} \tag{1}$$

are the apparent and real 4-dimensional Stokes vectors, respectively. $\mathbf{M}$ is the so-called Mueller matrix [*Mueller*, 1948]. In the simple case where real antennas are modeled as short dipoles, one can show that $\mathbf{M}$ decomposes in a product of two matrices $\mathbf{M}_{\text{ANT}}$ and $\mathbf{M}_{\text{DIR}}$, containing antenna properties (orientation and relative gain) and incoming direction of the observed point source, respectively.

[9] The Stokes parameters therefore can be derived as:

$$\mathbf{\Sigma} = \mathbf{M}_{\text{DIR}}^{-1} \cdot \mathbf{M}_{\text{ANT}}^{-1} \cdot \mathbf{\Sigma}_A. \tag{2}$$

[10] In Cassini's case, the antenna model matrix $\mathbf{M}_{\text{ANT}}$ was derived from in-flight antenna calibrations performed during the Jupiter flyby [*Vogl et al.*, 2004], and the antenna reference frame direction matrix $\mathbf{M}_{\text{DIR}}$ was derived from the

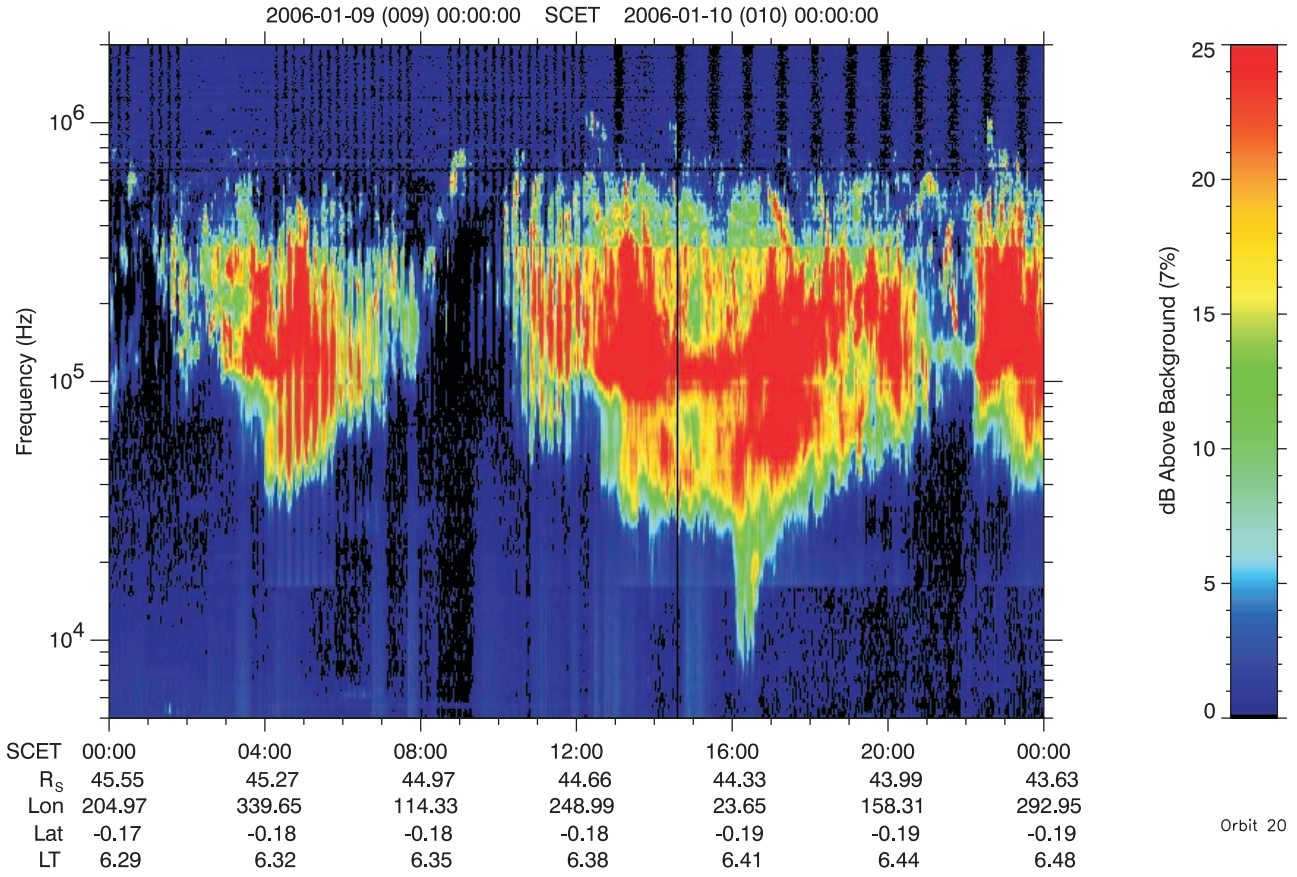

Figure 1. Dynamic spectrum recorded on 9 January 2006, by the RPWS experiment over the HFR frequency band, i.e., 3.5 kHz to 1.2 MHz. The color is associated to a relative intensity level where blue and red represent the instrumental background and the intense radio flux, respectively.

spacecraft ephemeris. In first approximation, the SKR radio emission can be assumed to come from one or several point sources with a linear degree of polarization equal to zero.

3. Phenomenology of SKR Envelope Spectra

3.1. Data Processing

[11] The present analysis of the SKR spectrum is based on observations performed by Cassini during the orbits 19 and 20 around Saturn; more particularly, the following days have been selected: 21, 22, and 23 December 2005, from 08 until 15, and from 18 until 23 January 2006, 01, 02 and 03 February 2006. From these RPWS/HFR observations, we have picked and chosen samples we consider to be representative of the SKR spectral shape. It is very tricky to define the upper and the lower limits of the SKR envelope over a given Saturnian rotation as one can see on the dynamic spectrum displayed in Figure 1. The highest frequencies are recorded at about 1 MHz but may decrease down to 600 kHz when the lowest frequencies are observed in the range 3.5–100 kHz. On the other hand, the observed SKR emissions result from the contribution of several sources located in both hemispheres. Also one can note that the frequency bandwidth, i.e., the difference between the maximum and the minimum frequencies varies significantly over durations of the order of a few minutes. As a consequence, it is not reasonable to estimate at each minute the frequency envelope variation because of the huge amount of data. So we have decided, as a first step, to consider the hourly dynamic spectra recorded by the RPWS experiment in the frequency range between 3.5 kHz and 1.2 MHz. Afterward we have estimated the polarization parameters of the radio wave, in particular the right-hand and left-hand circular components, using the Cassini/RPWS capabilities. This second step allows us to distinguish between the radio emissions coming from each hemisphere of the planet. In the following the calculated flux densities are actually electric field spectral densities; they are normalized to a distance of 50 Saturnian radii, and are expressed in $V^2\ m^{-2}\ Hz^{-1}$.

3.2. SKR Hourly Spectral Pattern

[12] Figure 2 shows 24 consecutive hourly spectral shapes of the SKR envelope observed on 09 January 2006. The flux density associated to the left-hand polarized component is displayed versus the observed frequency. In addition to the SKR spectra four curves are plotted, they designate the minimum, the median, the average and the maximum fluxes of the hourly observed spectra. The minimum and the maximum curves correspond to the levels 3% and 99% of the histogram of the flux density, respectively. More than two Saturnian rotations are visible in Figure 1: the first one spreads between 0000 SCET and 0900 SCET whereas the second one spreads between

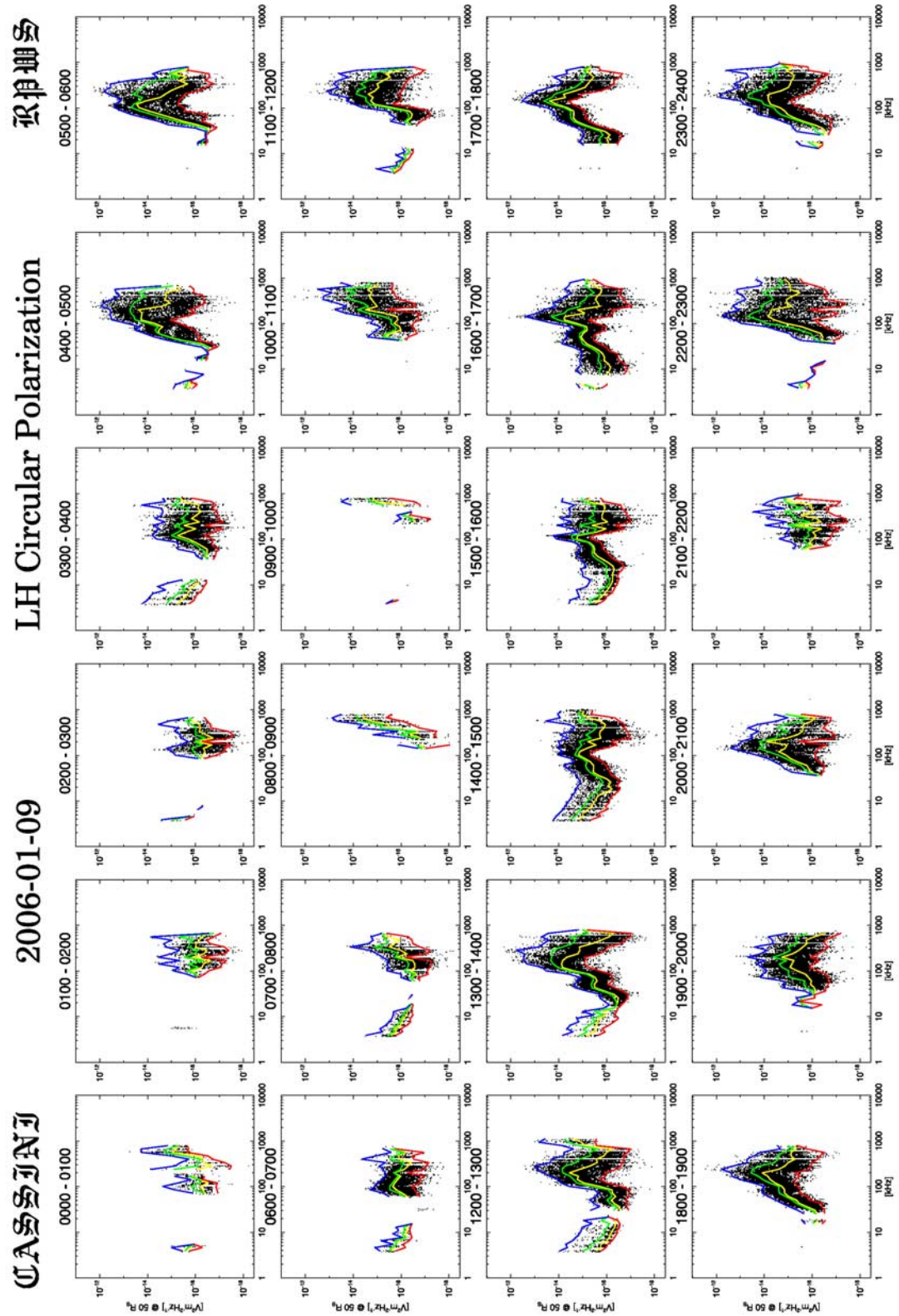

Figure 2. Sketch of hourly left-hand circular (LH) component spectra computed for the dynamic spectrum shown in Figure 1. Four curves which designate the minimum (red curve), the median (yellow curve), the average (green curve) and the maximum (blue curve) are superposed to the hourly SKR spectrum.

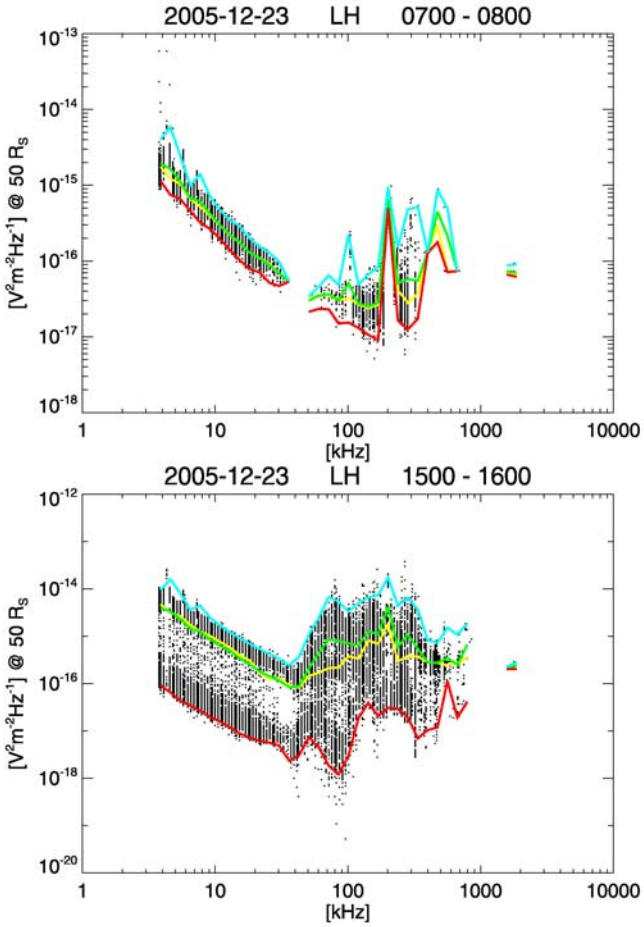

Figure 3. Component A of the SKR spectrum mainly observed in the frequency range from 3.5 kHz to 80–90 kHz. Examples display particular cases where this component has a thin (top panel) and thick (bottom panel) spectral shape.

1000 SCET and 2100 SCET. A third rotation starts at 2200 SCET. In Figure 2, one can notice that the flux density is weaker or the emission nearly absent between the rotations (e.g., at 0900–1000 SCET and 2100–2200 SCET). Most of the time, the envelope can be split up into three parts: a first one between 3–4 kHz and 70–80 kHz (component A), a second part between 70–80 kHz and 800–900 kHz (component B), and a third one (component C) between 800–900 kHz and 1200 kHz. In the following subsections, we describe the features of the SKR spectral envelope, where the component B represents the main part of the spectrum and the shape of which is typical of the SKR emission, as reported by the Voyager observations [*Kaiser et al.*, 1980]. This component will be compared to the theoretical SKR spectrum computed by *Galopeau et al.* [1989].

3.2.1. Component A

[13] This component is mainly observed at the lower frequencies of the spectrum and up to ~80 kHz. The shape usually exhibits a negative slope which means a decrease of the flux density when the frequency varies from 3.5 kHz to 80 kHz. Two types of shapes can be distinguished: thin (see example in Figure 3 top) and thick which is the most often observed feature (see example in Figure 3 bottom). The component A appears disconnected from the component B in the beginning of (see example in Figure 4 top) and during (see example in Figure 4 bottom) the Saturnian rotation. Also in some cases, the component A is totally absent from Saturn's spectrum as shown in Figure 2 in the time intervals 1000–1100 SCET and 1700–1800 SCET. The flux density reaches values of the order of 10^{-14} V^2 m^{-2} Hz^{-1}. Rarely the flux density of the component A appears more intense than that of the component B as it can be seen in Figure 3 bottom.

3.2.2. Component B

[14] The component B is the most powerful component of the Saturnian radio emission spectrum in the frequency range between 80–90 kHz and 900 kHz. The flux density, normalized to 50 Saturnian radii, attains values of about 10^{-11} V^2 m^{-2} Hz^{-1}, i.e., two or three orders of magnitude more intense than the other components. The envelope shows a rapid increase in flux density up to frequencies between 100 kHz and 200 kHz, followed by a decrease in flux toward 800–900 kHz (see Figure 5). The general shape of the component B envelope is almost symmetrical around 150 kHz. However, the envelope displays sometimes different shapes with more than one maximum. Examples of

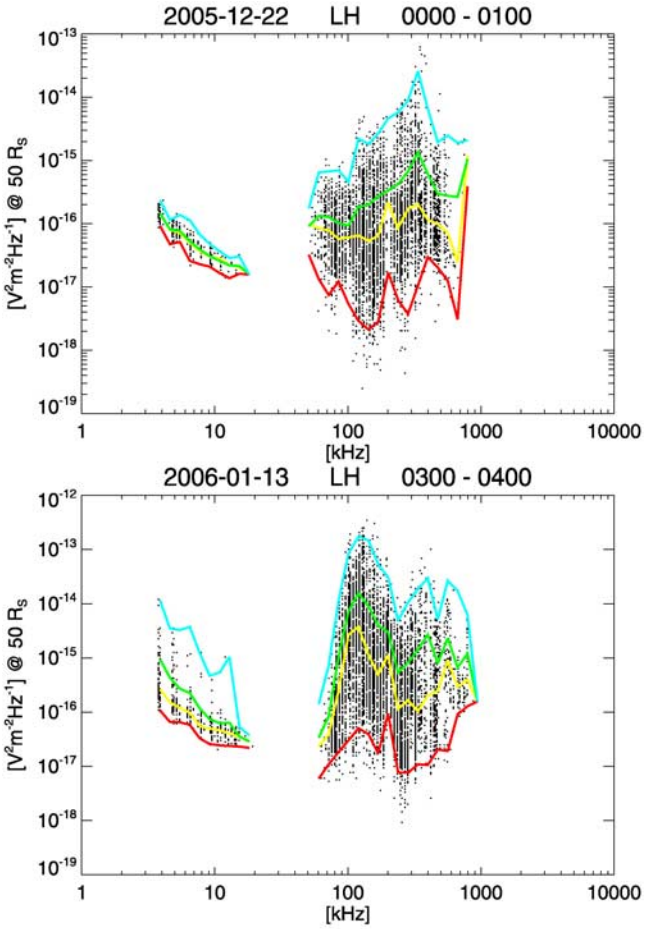

Figure 4. Cases of hourly SKR spectra where components A and B are disconnected.

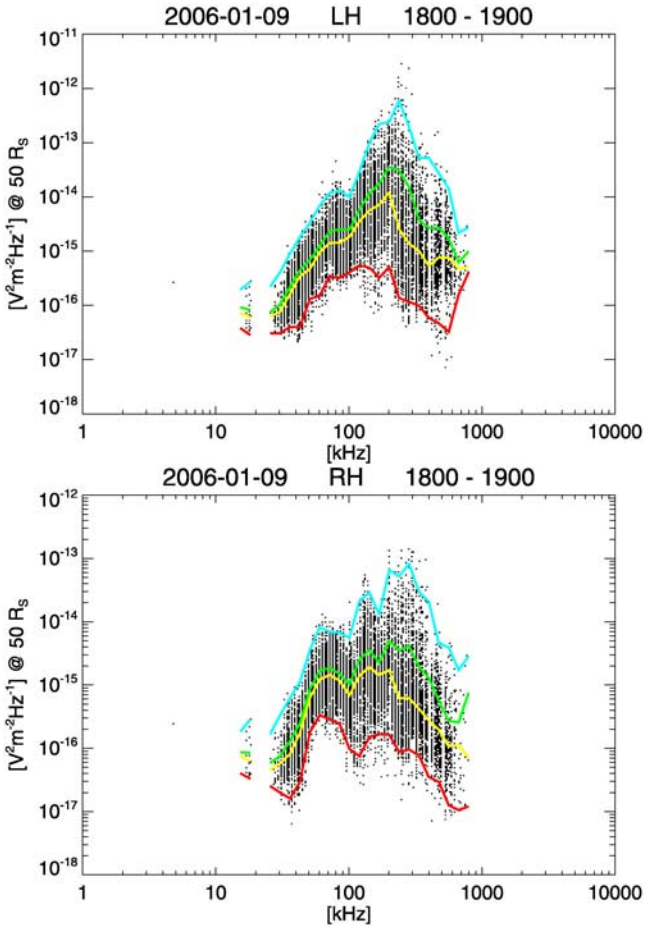

Figure 5. 'Classic' well known component of SKR spectrum, called component B, observed on 9 January 2006, in both circular polarizations (left- and right-hand). Note that the intensity level of the right-hand emissions is one order of magnitude more important.

the component B envelope with several intensity peaks are shown in Figure 6.

3.2.3. Component C

[15] As described in the previous subsection the component B presents, after a maximum at about 200 kHz, a decrease of the flux density which corresponds to the cut-off of the SKR emission. However, in some cases one notes an increase again of the radiation beyond ~900 kHz, which reaches a maximum at 1 MHz, followed by a fall of the emission around 1.2 MHz. This last part of the SKR envelope is called hereafter component C as it is shown in Figure 7.

3.3. Spectral Polarization of SKR Emission

[16] For the polarization study we consider the Saturnian kilometric radiation observed during one given day, i.e., 09 January 2006. As it is described later on we first estimate the Stokes parameters in the frequency band from 3.5 kHz to 1.2 MHz and then we derive the corresponding histograms. Afterward we calculate the circular (P_c), the linear (P_l), and the total (P) degrees of polarization and the corresponding flux densities, taking into consideration only the data for which the computed total degree of polarization is in the range [0, +1].

3.3.1. Stokes Parameters

[17] Figure 8 shows the variation of the Stokes parameters (S, Q, U, V) versus the observed frequency. The flux density S varies between 10^{-17} V^2 m^{-2} Hz^{-1} and 10^{-11} V^2 m^{-2} Hz^{-1}

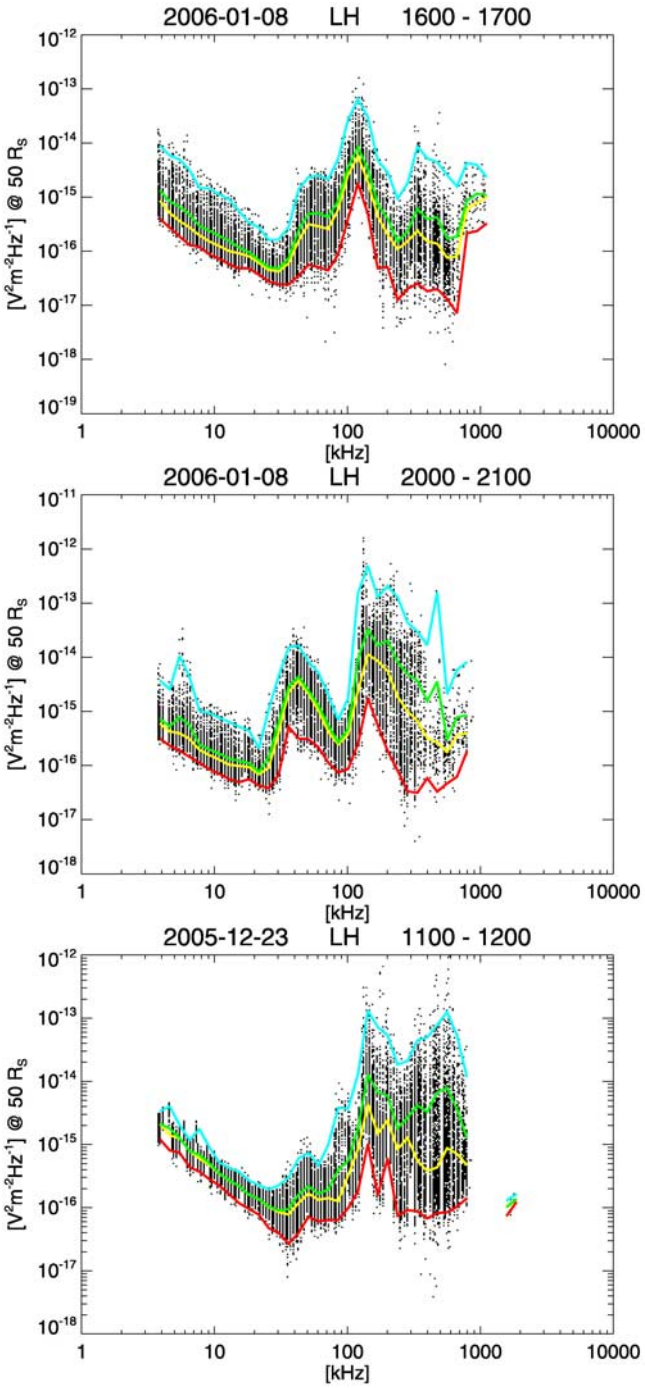

Figure 6. Variability of the SKR 'classic' spectrum where only one maximum is observed at low (between 40 kHz and 200 kHz) and high (between 100 kHz and 900 kHz) as it is shown in the top and bottom panels, respectively. Sometimes both maxima are observed (middle panel).

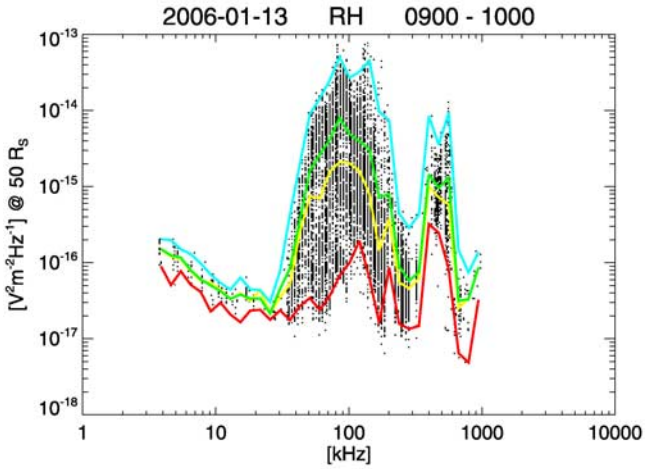

Figure 7. The component C of the SKR spectrum principally appears in the frequency range from 800–900 kHz to 1.2 MHz. It follows the component B and was also observed during the Voyager mission.

with a maximum at about 200 kHz. The histogram of the circular component V displays two peaks, one significant around zero and a second one smaller around the value -1. The linear components, i.e., Q and U, present similar variations over the whole spectrum with an average value around zero as one can see on the corresponding histograms. However, a detailed analysis shows that at low (3.5–70 kHz) and high (500–1200 kHz) frequencies the two components have random variations with values smaller than -1 and bigger than +1. In the frequency range between 70 kHz and 500 kHz both linear components Q and U are nearly equal to zero. According to this analysis, the SKR emission is mainly circularly polarized. However, the parameter Q presents a weak linear component and V attains the value -1 only in the frequency range from 70 kHz to 500 kHz.

3.3.2. Polarization State

[18] We select the data for which the total degree of polarization is less than or equal to 1. The aim is to neglect the aberrant polarization values discovered in the previous subsection. Figure 9 shows the polarization state illustrated by the total (P), the circular (P_c) and the linear (P_l) degrees of polarization. We also estimate the position angle (PA) of the major axis of the polarization ellipse for the data satisfying to the condition $P_l > 0.3$. It comes that a little part of the emission (less than 20%) has a polarization degree of $\sim$1. The degree of linear polarization is mainly less than 0.2 with a very weak part around +1. The parameter PA is mostly around 0° which is in agreement with a weak linear component. The degree of circular polarization is principally equal to -1 but for some event cases P_c is equal to +1 or 0.

[19] The investigation of the flux density is shown in Figure 9 (right panels) for the following parameters: total intensity S, left-hand (LH), right-hand (RH), and linear (L) components. The total flux density S is displayed in Figure 8 (left column, top panel) and Figure 9 (right column, top panel); the latter being restricted to data fulfilling $P \leq 1$. By comparing both figures one notes that: (1) the emission at frequencies higher than $\sim$900 kHz is absent in Figure 9, and (2) the spectrum at low frequency (below 50 kHz) is very dense in Figure 8. On the other hand, the left- and right-hand flux densities (LH and RH in Figure 9) present different spectral shapes of the SKR envelope. Hence the peaks can be different from one polarization to the other one at a given time. In general the emission corresponding to the right-hand circular component is dominant as it can be seen in the previous figures. Therefore the maximum at about 200 kHz is clearly seen on the RH polarized spectrum.

3.3.3. Summary of the Main Results

[20] Our analysis leads us to the first conclusion that the SKR envelope is very unpredictable and variable, and the timescales involved extend over a large range, from hours to days. The separation between the polarizations (right- and left-hand) does not help to estimate the exact value of the corresponding frequency bandwidth. However, we classify the entire SKR envelope observed between 3.5 kHz and 1.2 MHz in three components. The polarization investigation gives us an estimation of the change from one component to the next. Hence a linear component, less than 10% of the emission, seems to be the main polarization feature of the components A and C. The circular polarization is observed in the frequency range from 80–90 kHz to 900 kHz which corresponds to the component B. Generally it comes from our analysis that only part (less than 20%) of the spectra observed by the HFR is totally circularly polarized.

4. Discussion

[21] The Saturnian kilometric emissions present variable low and high frequency boundaries. The analysis of the hourly spectral shape leads us to classify and to characterize the SKR envelope. Some of our findings are in concurrence with previous Voyager investigations and others not. We start in the next subsection to recall and reexamine the main characteristics of the model developed by *Galopeau et al.* [1989] with the aim to study the origin of the shape of the SKR spectrum. Then we confront the irregularity of the SKR bandwidth of the different components with the analysis by *Genova et al.* [1983] where some spectral features might be comparable. Finally we attempt to give an answer to the question of the precise degree of circular polarization and the existence, or not, of weak linear component.

4.1. Return on Theoretical Model of SKR Spectrum

[22] A theoretical model of Saturn's kilometric radiation spectrum was computed by *Galopeau et al.* [1989]. The authors based their model on the cyclotron maser instability mechanism which is supposed to be at the origin of most non-thermal planetary radio emissions. It is a resonant coupling between X-mode waves and an electron population characterized by a positive gradient in perpendicular velocity of the distribution function ($\partial f/\partial v_\perp > 0$). The CMI leads to a direct amplification of the waves when the following resonance condition is fulfilled:

$$\omega - k_\parallel v_\parallel - \frac{\omega_c}{\gamma} = 0 \qquad (3)$$

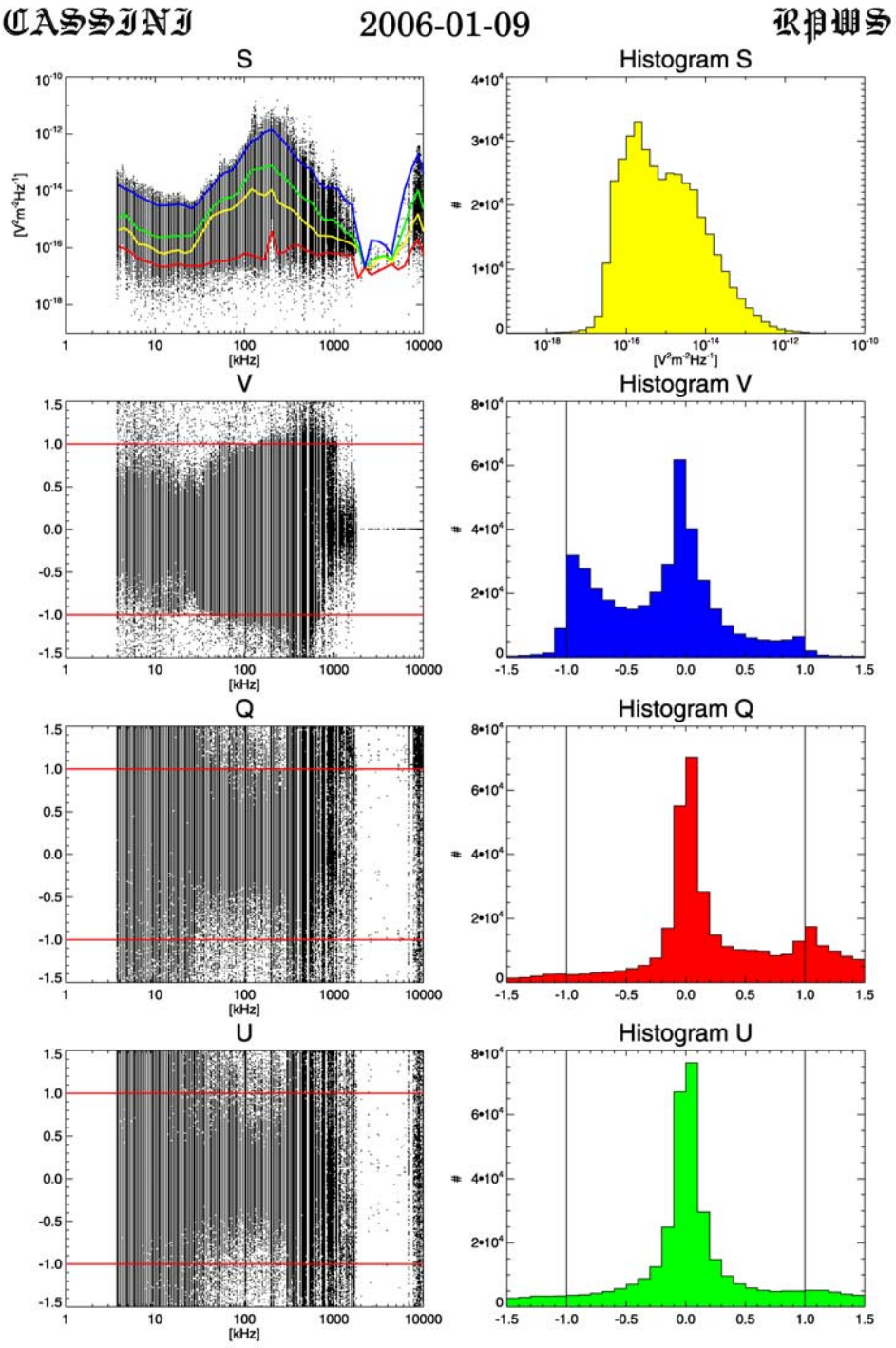

Figure 8. Stokes parameters (S, V, Q, U) of SKR emissions versus frequency (left-panels) and corresponding histograms (right-panels) recorded on 9 January 2006. The top left-panel shows four types of spectra similar to those proceeded in the Figure 2. The horizontal (left-panels) and vertical (right-panels) lines indicate the aberrant polarization measurements of V, Q, and U which are smaller and higher than ±1.

where ω and $k_{||}$ are the pulsation and the parallel wave vector of the waves and $v_{||}$ and γ the parallel velocity and Lorentz factor of the electrons. Considering that the wavelength of the SKR is comparable with the gradient length of the magnetic field, a theory of the CMI in inhomogeneous medium was required. As a consequence, a necessary condition for the waves to be amplified is:

$$\varepsilon = \left(\frac{f_p}{f_c}\right)^2 < 0.148 \tag{4}$$

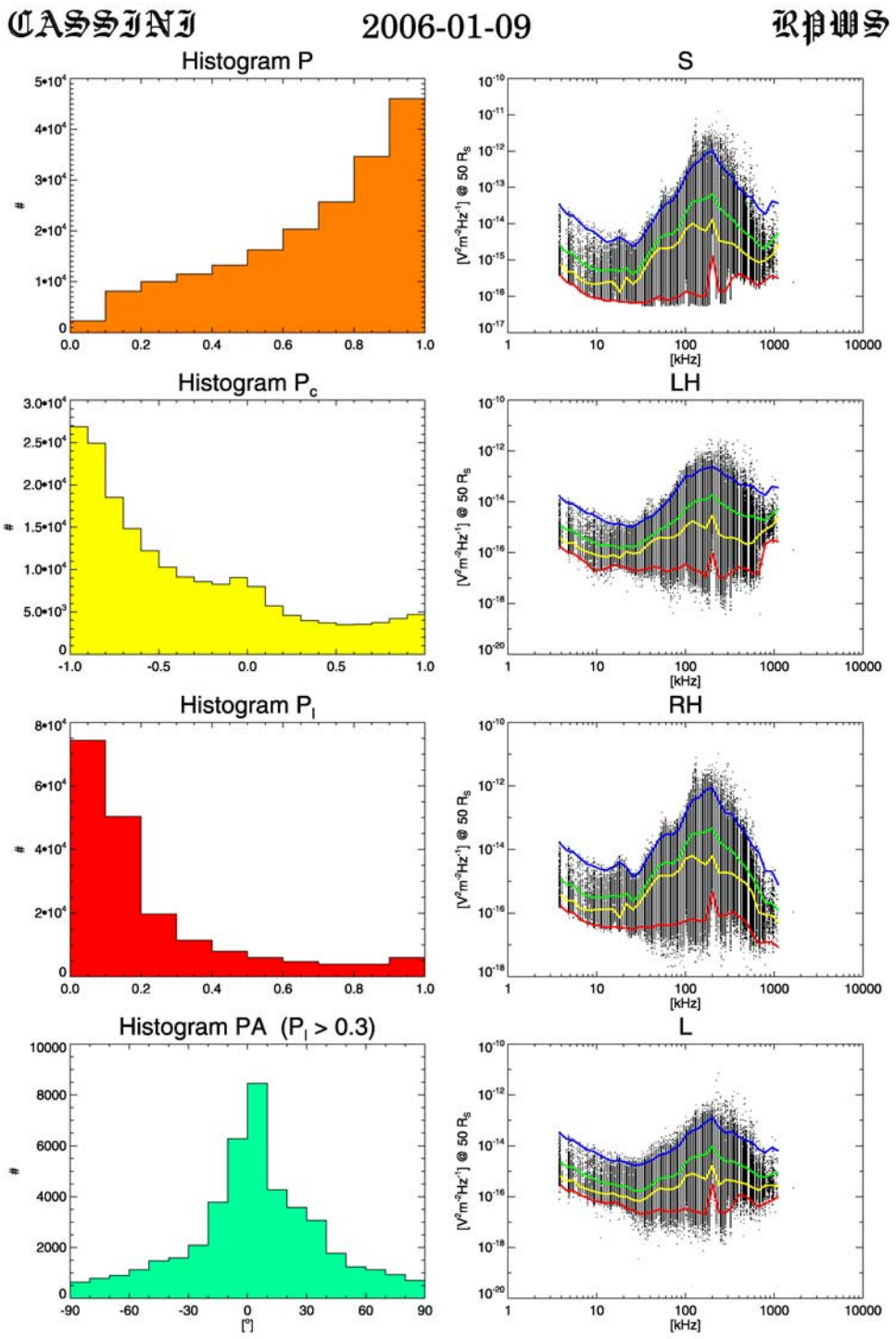

Figure 9. Histograms of the degree of the total (P), the circular (P_c) and linear (P_l) polarizations of the event of Figure 8. In this case only data satisfying the condition ($Q^2 + U^2 + V^2$) ≤ 1 are taken into consideration. The total (S), left-hand (LH), right-hand (RH) and linear (L) flux densities are displayed versus frequency. The fluxes are normalized to a distance of 50 R_S. The histogram of the distribution of the position angle of the linear component is also displayed for $P_l > 0.3$.

where f_p and f_c are the plasma- and the gyrofrequency, respectively. The model by *Galopeau et al.* [1989] is a maximum spectrum which can be compared with the envelope spectra (corresponding to the level 99% of the histogram of the flux density) presented in this study (see Figures 8 and 9). The authors supposed that the amplification of the waves reached a saturation level. They also considered optimum conditions for the source size of the radiation filling an entire magnetic flux tube. Finally their model of SKR spectrum only depends on macroscopic

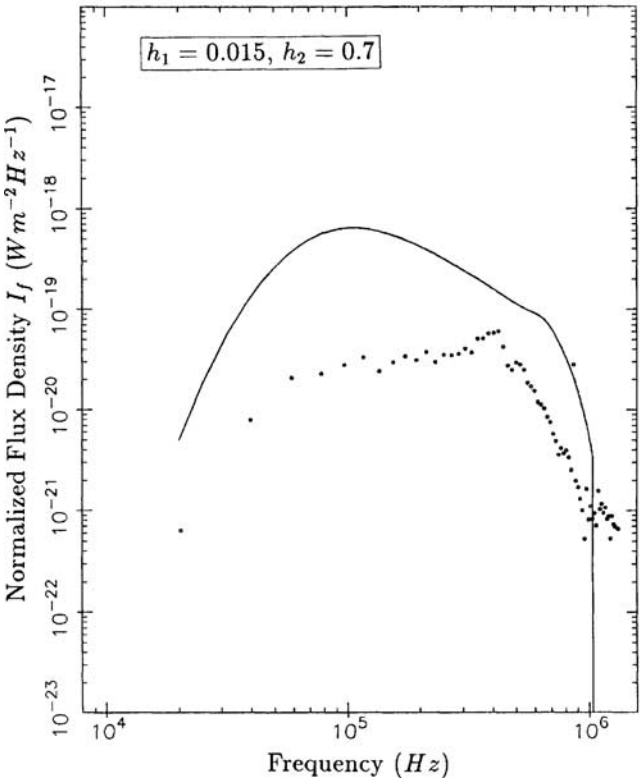

Figure 10. Theoretical SKR spectrum (solid curve) calculated by *Galopeau et al.* [1989, Figure 8]. It corresponds to a nonlinearly saturated emission by trapping, amplified by the cyclotron maser instability mechanism. This maximum spectrum is compared to the typical 1% level SKR spectrum (circles) observed by Voyager 1, before the encounter with Saturn, on 31 October 1980. The flux densities, in W m^{-2} Hz^{-1}, are normalized to a 1-AU distance. h_1 and h_2 are the values of the scale heights of the plasma density model used for the calculation.

parameters of the Saturnian environment, in particular the magnetic field and the plasma density.

[23] The plasma distribution model used by *Galopeau et al.* [1989, Figure 3 in their paper] is the sum of an ionosphere and a plasma disc characterized by scale heights h_1 and h_2, respectively. Then, in coordinates (r, z), where r is the radial distance from the center of Saturn and z the distance from the equatorial plane, the plasma density is:

$$n = n_{10} \exp\left[-\frac{R_S}{h_1}\left(1 - \frac{R_S}{r}\right)\right] + n_{20} L^{-3} \exp\left[-\left(\frac{z}{h_2}\right)^2\right]. \quad (5)$$

[24] For values of h_1 and h_2 in agreement with Voyager's observations the authors computed a maximum spectrum displayed in Figure 10. The cut-off of the spectrum at high frequencies is directly linked to the fact that the CMI mechanism does not work for $(f_p/f_c)^2 > 0.148$, whereas the decrease toward low frequencies results from the rarefaction of the plasma far from Saturn. The comparison of the theoretical spectrum by *Galopeau et al.* [1989] with the spectral envelopes determined from Cassini/RPWS measurements allows us to access to the parameters of the plasma and of the magnetic field surrounding Saturn. Correlations will be possible with other parameters measured by the spacecraft, notably the solar wind parameters.

4.2. Irregularity of the SKR Frequency Bandwidth

[25] The first important outcome of our analysis is the unpredictability and variability of the SKR envelope. Despite the presence of some kinds of emissions as reported by *Genova et al.* [1983] or as described in our study it is not possible to accurately define and estimate the exact spectral SKR envelope. However, it is clearly shown in our investigation of the SKR spectrum that we deal with different components which are directly, or not, linked to Saturn's auroral regions. The shape of the component B is very similar and comparable to the envelope of the observed spectrum (see Figure 10) and is also typical of the auroral emissions. It can be regarded as a mixture of the high and the low components as also found by *Genova et al.* [1983] but limited to the frequency range from 80–90 kHz to 900 kHz. This is clearly seen in the selected examples where only the lower (see Figure 6 top) or the higher (see Figure 6 middle) parts of the component B is observed. In some cases both kinds are observed before and after the maximum of the spectrum, i.e., in the range 100–200 kHz (see Figure 6 bottom). However, the usually observed spectral shape of the component B seems to be the superposition of the two kinds of emissions. On the other hand, as it is shown in the previous section, the degree of circular polarization is the same in the component B frequency range where both emission kinds are observed. One could conclude that they are emitted from the same hemisphere but not from the same source region.

[26] The components A and C are found with a weak degree of linear polarization (about 20%) which can suggest that they are surely different from the component B. However, the component C is certainly generated in Saturn's auroral region where high frequencies (more than 900 kHz) are observed, like component B. According to *Galopeau et al.* [1989], the cut-off of the spectrum at high frequencies is directly due to the value of the ratio $(f_p/f_c)^2$ which is greater than 0.148. This is the case of the component B which decreases at high frequency. However, one has to explain why the emission increases again (after 900 kHz), attains a maximum, and falls down again at frequency about 1.2 MHz. If one supposes that the components B and C have a same origin, one has to elucidate why the polarization state changes from circular to elliptical.

[27] The component A is the most confusing because its shape is different from the classic spectrum. It is evident that the origin of the components A and C are distinct despite a common linear polarization feature. The low frequency range of the component A (3–70 kHz) is probably due to the fact that the emissions are generated in the auroral region at large distance compared with the components B and C. The particles that are at the origin of the components B and C are probably located at auroral high latitudes, while the particles responsible for the component A may come from inner areas of Saturn's magnetosphere, like the plasma disk, the rings or the satellites.

4.3. Possible Presence of Elliptical Polarization

[28] It is very tricky to give an interpretation to the measured SKR polarization, in particular the linear one. Despite the calibration method described in section 2, more than 50% of the observed emissions have a degree of circular polarization less than one. If one supposes that the SKR is fully circularly polarized (which would be in agreement with an emission generated by the CMI) it is difficult to explain the measured SKR polarization. Two major causes could be at the origin of this discrepancy, an inaccurate estimation of all factors which contribute to the calculation of the polarization or a real natural effect which only occurs in Saturn's magnetosphere.

[29] The estimation of the polarization state of a radio wave is well-known in the case of ground [*Kraus*, 1966] and space [*Lecacheux*, 1978] observations. However, several papers reported a real complexity to estimate the correct state of polarization of the radio wave because only two principal parameters were measured, i.e., the intensity S and the sense of circular polarization V. In the case of the Voyager mission, *Ortega-Molina and Lecacheux* [1990] used the SKR radiation as a calibration source with the aim to reduce the uncertainty from 30% to 5% of the degree of circular polarization. Several sources of error are listed, in particular those linked to the signal-to-noise ratio which might be at the origin of the discrepancy between the observations and theory.

[30] More recently *Cecconi et al.* [2006] reported a SKR polarization study based on data recorded by the RPWS/HFR experiment six months before the encounter with the planet (in July 2004). The authors considered three frequency bands (i.e., LF (10–100 kHz), MF (100–325 kHz) and HF (325–1200 kHz)) and selected for each band 0.3%, 0.02% and 0.005% of the total data, respectively. *Cecconi et al.* [2006] do not make clear the grounds of this division in the HFR frequency range. They found a reasonable degree of total polarization which is less than one, and weak linear component in the frequency range 325–1200 kHz. This linear polarization feature is considered as an artifact due to both interference lines and a small number of selected data. Our results cannot be combined to the previous one because the analyzed period and the selected frequency bandwidth are different. Despite this discrepancy, it clearly appears from both studies that more investigations should be done before giving a precise explanation for the 'missed' data. *Cecconi et al.* [2006] simply considered less than 1% of the total observed samples. In the framework of our analysis we also show that only an insignificant part of the SKR emissions are 100% polarized. Of course both data sets were first calibrated with the aim of reducing the background receiver effect, of estimating the effective height of the antenna and of correcting the observed data from the maneuvers of the spacecraft.

5. Conclusion

[31] The visit to the planet Saturn by the Cassini mission gives a good opportunity to re-investigate the properties of the Saturnian kilometric radiation, in particular its spectral shape. The SKR envelope appears to be very variable in timescales of one hour, one Saturnian rotation or one day. We proceed to the calibration of the HFR data observed by the RWPS experiment taking into consideration several factors like the signal-to-noise ratio and, in particular, the observation conditions (effect of the galactic background, antenna reception system, observation modes, spacecraft maneuvers). The analysis of the emission spectral shape leads to discern three components. Most of the time the SKR emission covers only part of the HFR frequency range between 70–80 kHz and 800–900 kHz. Two others components appear to be different from the 'classic SKR' because of their spectral shapes and also their corresponding polarizations. The derived Stokes parameters have allowed us to distinguish between the radiations coming from the northern and southern hemispheres using the sense of circular polarization. The 'classic SKR' radiation seems to be circularly polarized when the two others components present a weak linear polarization. The origin of these emissions is linked to the auroral region where they are generated, nevertheless the unpredictability and the variability of the spectral shape are still subject of investigation. A statistical analysis should give more explanation about the relationship between these components and the way how they act together.

[32] **Acknowledgments.** The authors would like to express their sincere thanks to all members of the RPWS experiment, especially to the project managers D. A. Gurnett and W. S. Kurth. This work was supported by grants from the EuroPlaNet project.

[33] Amitava Bhattacharjee thanks Donald Gurnett for his assistance in evaluating this paper.

References

Boudjada, M. Y., and F. Genova (1991), The left-hand polarization sense of the Jovian decameter radiation, *Astron. & Astrophys. Suppl. Ser.*, *91*, 453–467.

Boudjada, M. Y., P. H. M. Galopeau, H. O. Rucker, and A. Lecacheux (2000), Jovian narrow-band as generator of the jovian millisecond radio bursts, *Astron. & Astrophys.*, *363*, 316–322.

Burke, B. F., and K. L. Franklin (1955), Observations of a variable radio source associated with planet Jupiter, *J. Geophys. Res.*, *60*, 213–217.

Cecconi, B., P. Zarka, and W. S. Kurth (2006), SKR polarization and source localization with the Cassini/RPWS/HFR instrument: First results, in *Planetary Radio Emissions VI*, edited by H. O. Rucker, W. S. Kurth, and G. Mann, pp. 37–49, Austrian Academy of Sciences Press, Vienna.

Desch, M. D. (1982), Evidence for solar wind control of Saturn radio emission, *J. Geophys. Res.*, *87*, 4549–4554.

Desch, M. D., and H. O. Rucker (1983), The relationship between Saturn kilometric radiation and the solar wind, *J. Geophys. Res.*, *88*, 8999–9006.

Galopeau, P. H. M. (1992), Source location of the Saturnian kilometric radiation, in *Planetary Radio Emissions III*, edited by H. O. Rucker, S. J. Bauer, and M. L. Kaiser, pp. 231–240, Austrian Academy of Sciences Press, Vienna.

Galopeau, P., P. Zarka, and D. Le Queau (1989), Theoretical model of Saturn's kilometric radiation spectrum, *J. Geophys. Res.*, *94*, 8739–8755.

Galopeau, P., P. Zarka, and A. Ortega-Molina (1991), Evidence of Saturn's magnetic field anomaly from saturnian kilometric radiation high-frequency limit, *J. Geophys. Res.*, *96*, 14,129–14,140.

Genova, F. (1985), Source location of planetary radio-emissions, in *Planetary Radio Emissions*, edited by H. O. Rucker and S. J. Bauer, pp. 51–71, Austrian Academy of Sciences Press, Vienna.

Genova, F., and M. G. Aubier (1987), High frequency limit and visibility of the non-Io and Io-dependent Jovian decameter radio emission, *Astron. & Astrophys.*, *177*, 303–309.

Genova, F., B. M. Pedersen, and A. Lecacheux (1983), Dynamic spectra of Saturn kilometric radiation, *J. Geophys. Res.*, *88*, 8985–8991.

Gurnett, D. A., et al. (2004), The Cassini radio and plasma wave investigation, *Space Sci. Rev.*, *114*, 395–463, doi:10.1007/s11214-004-1434-0.

Hamaker, J. P., J. D. Bregman, and R. J. Sault (1996), Understanding radio polarimetry. I. Mathematical foundations, *Astron. & Astrophys. Suppl. Ser.*, *117*, 137–147.

Kaiser, M. L., and M. D. Desch (1984), Radio emissions from the planets Earth, Jupiter, and Saturn, *Rev. Geophys. Space Phys.*, *22*, 373–384.

Kaiser, M. L., M. D. Desch, J. W. Warwick, and J. B. Pearce (1980), Voyager detection of nonthermal radio emission from Saturn, *Science*, *209*, 1238–1240.

Kaiser, M. L., M. D. Desch, W. S. Kurth, A. Lecacheux, F. Genova, B. M. Pedersen, and D. R. Evans (1984), Saturn as a radio source, in *Saturn*, edited by T. Gehrels and M. S. Matthews, pp. 378–415, Univ. of Arizona Press, Tucson.

Kraus, J. D. (1966), *Radio Astronomy*, McGraw-Hill Book Company, New York.

Kurth, W. S., D. A. Gurnett, and F. L. Scarf (1981a), Control of Saturn's kilometric radiation by Dione, *Nature*, *292*, 742–745.

Kurth, W. S., D. A. Gurnett, F. L. Scarf, R. L. Poynter, and J. D. Sullivan (1981b), Voyager observations of Jupiter's distant magnetotail, *J. Geophys. Res.*, *86*, 8402–8412.

Lecacheux, A. (1978), Direction finding of a radiosource of unknown polarization with short electric antennas on a spacecraft, *Astron. & Astrophys.*, *70*, 701–706.

Lecacheux, A. (2001), Radio observations during the Cassini flyby of Jupiter, in *Planetary Radio Emissions V*, edited by H. O. Rucker, M. L. Kaiser, and Y. Leblanc, pp. 1–14, Austrian Academy of Sciences Press, Vienna.

Lecacheux, A. (2005), Solar type III burst analysis with Cassini/RPWS: Lessons for Stereo, paper presented at Solar Orbiter and Stereo meeting, Graz, Austria, 28 –29 November .

Lecacheux, A., M. Y. Boudjada, H. O. Rucker, J. L. Bougeret, R. Manning, and M. L. Kaiser (1998), Jovian decameter emissions observed by the Wind/WAVES radioastronomy experiment, *Astron. & Astrophys.*, *329*, 776–784.

Mueller, H. (1948), The foundation of optics, *J. Opt. Soc. America*, *38*, 661.

Ortega-Molina, A., and A. Lecacheux (1990), Polarization response of the Voyager-PRA experiment at low frequencies, *Astron. & Astrophys.*, *229*, 558–568.

Vogl, D. F., et al. (2004), In-flight calibration of the Cassini-Radio and Plasma Wave Science (RPWS) antenna system for direction-finding and polarization measurements, *J. Geophys. Res.*, *109*, A09S17, doi:10.1029/2003JA010261.

Warwick, J. W., D. R. Evans, J. H. Romig, J. K. Alexander, M. D. Desch, M. L. Kaiser, M. G. Aubier, Y. Leblanc, A. Lecacheux, and B. M. Pedersen (1982), Planetary radio astronomy observations from Voyager 2 near Saturn, *Science*, *215*, 582–587.

Wu, C. S., and L. C. Lee (1979), A theory of the terrestrial kilometric radiation, *Astrophys. J.*, *230*, 621–626.

M. Y. Boudjada, Abteilung für Physik des erdnahen Weltraums, ÖAW-Forschungszentrum Graz, Schmiedlstraße 6, A-8042, Graz, Austria. (mohammed.boudjada@oeaw.ac.at)

P. H. M. Galopeau, Centre d'Étude des Environnements Terrestre et Planétaires, 10–12 Avenue de l'Europe, F-78140 Vélizy, France. (patrick.galopeau@cetp.ipsl.fr)

A. Lecacheux, Observatoire de Paris, LESIA, 5 Place J. Janssen, F-92195 Meudon, France. (alain.lecacheux@obspm.fr)